

# 1 Observation of Energetic particles between a pair of Corotating 2 Interaction Regions

3 Z. Wu<sup>1</sup>, Y. Chen<sup>1</sup>, G. Li<sup>2,\*</sup>, L. L. Zhao<sup>2</sup>, R. W. Ebert<sup>3</sup>, M. I. Desai<sup>3,4</sup>, G. M. Mason<sup>5</sup>, B.  
4 Lavraud<sup>6</sup>, L. Zhao<sup>7</sup>, Y. C.-M. Liu<sup>8</sup>, F. Guo<sup>9</sup>, C. L. Tang<sup>1</sup>, E. Landi<sup>7</sup>, J. Sauvaud<sup>6</sup>

5 <sup>1</sup> Institute of Space Sciences and School of Space Science and Physics, Shandong University  
6 at Weihai, Weihai, China 264209

7 <sup>2</sup> Department of Space Science and CSPAR, University of Alabama in Huntsville 35899,  
8 USA

9 <sup>3</sup> Southwest Research Institute, San Antonio, TX, USA

10 <sup>4</sup> University of Texas at San Antonio, San Antonio, TX, USA

11 <sup>5</sup> Applied Physics Laboratory, Johns Hopkins University, Laurel, MD, USA

12 <sup>6</sup> Institut de Recherche en Astrophysique et Planétologie, Université de Toulouse (UPS),  
13 Toulouse, France. and Centre National de la Recherche Scientifique, UMR 5277, Toulouse,  
14 France

15 <sup>7</sup> Department of Atmospheric, Oceanic, and Space Sciences, University of Michigan, Ann  
16 Arbor, MI, USA, 48105

17 <sup>8</sup> State Key Laboratory of Space Weather, National Space Science Center, CAS. Beijing,  
18 China 100190

19 <sup>9</sup> Theoretical Division, Los Alamos National Laboratory, NM, USA

20 \* gang.li@uah.edu

21 Received \_\_\_\_\_; accepted \_\_\_\_\_

## ABSTRACT

We report observations of the acceleration and trapping of energetic ions and electrons between a pair of corotating interaction regions (CIRs). The event occurred in Carrington Rotation 2060. Observed at spacecraft STEREO-B, the two CIRs were separated by less than 5 days. In contrast to other CIR events, the fluxes of energetic ions and electrons in this event reached their maxima between the trailing-edge of the first CIR and the leading edge of the second CIR. The radial magnetic field ( $B_r$ ) reversed its sense and the anisotropy of the flux also changed from sunward to anti-sunward between the two CIRs. Furthermore, there was an extended period of counter-streaming suprathermal electrons between the two CIRs. Similar observations for this event were also obtained for ACE and STEREO-A. We conjecture that these observations were due to a “U-shape” large scale magnetic field topology connecting the reverse shock of the first CIR and the forward shock of the second CIR. Such a disconnected U-shaped magnetic field topology may have formed due to magnetic reconnection in the upper corona.

## 1. Introduction

Corotating interaction regions (CIRs) are commonly found during solar minimum. They are formed when fast solar wind (often from coronal holes) overtakes slow solar wind (often from near a streamer belt) (Kreiger et al. 1973; Feldman et al. 1981; Gosling et al. 1981). Because the slow and fast winds are two plasmas of different magnetic origin, there is a stream interface between them and two shock waves can form with a forward shock propagating into the slow wind and a reverse shock propagating into the fast wind (but

31 both carried outwards by the solar wind) (Smith & Wolfe 1976; Pizzo 1985). The shock  
32 waves are often formed beyond 1 AU (Smith & Wolfe 1976; Pizzo 1985). However, recent  
33 studies showed that CIR shocks can form as close as 0.7 AU (Jian et al. 2006).

34 CIRs and the associated shocks are a major source of energetic particle acceleration in  
35 the interplanetary medium; (e.g., Van Hollebeke (1981); Tsurutani et al. (1982)). Indeed,  
36 during solar minimum when the coronal mass ejection (CME) rate is low, CIRs are the  
37 dominant source of energetic particles in the interplanetary medium at 1 AU (for recent  
38 reviews; see, e.g., Fisk & Jokipii (1999); Gosling & Pizzo (1999); Mason & Sanderson  
39 (1999); Scholer (1999); Richardson (2004)). These energetic particles have approximately a  
40 solar wind composition up to a few MeV nucleon<sup>-1</sup>, and sometimes to 10-20 MeV nucleon<sup>-1</sup>,  
41 indicating that they are accelerated from the solar wind (e.g. Mason & Sanderson  
42 (1999)). However, examination of particles such as He<sup>+</sup> and <sup>3</sup>He showed that they  
43 are more abundant in the CIRs than in the uncompressed solar wind, suggesting that  
44 the interplanetary suprathermal ion pool also contributes (e.g., Gloeckler et al (1994);  
45 Mason et al (2000); Möbius et al (2002); Mason et al. (2008a)). Furthermore, recent  
46 observations by Mason et al. (2012) found that the heavy ion abundances show a clear  
47 correlation with sunspot number, where heavy ions are more enhanced during active periods.  
48 Although the acceleration likely occurs at CIR shocks, how the population of seed particles  
49 is injected into the shock remains not well understood. Electrons are also accelerated to  
50 several hundred keV in CIRs, particularly at distances beyond 1 AU. (Simnett & Roelof  
51 1995; Simnett 2003).

52 The peak fluxes in CIRs often occur at the reverse and forward shocks, with fluxes  
53 at the reverse shock generally being larger (Heber et al. 1999; Mason & Sanderson 1999).  
54 For example, in a recent survey of 50 CIRs between 2007 February and 2008 September,  
55 Bučík et al. (2009b) found that in 90% of the events the peak flux of energetic helium

56 occurred within the compressed region or the trailing edge. In the remaining 10% of the  
57 events, the peak flux occurred within 24 hours of the trailing edge. Ebert et al. (2012)  
58 also confirmed this result. Note that even if there are no shocks associated with the CIRs,  
59 as long as there is significant local compression near the CIRs, particles are subject to  
60 acceleration (Desai et al. 1998; Giacalone et al. 2002). Indeed, Desai et al. (1998) showed  
61 that, for CIRs near 5 AU, the local compression ratio was a key factor in determining the  
62 intensity of 1 MeV protons, regardless of whether or not the CIR was bounded by shocks.  
63 Ebert et al. (2012) showed a similar result for  $< 0.8$  MeV/nucleon Helium ions for CIRs at  
64 1 AU.

65 The solar wind suprathermal electron population (in the 70 to 2000 eV range) is  
66 typically made of the “halo” population (generally tenuous and isotropic) and the “strahl”,  
67 an intense beam of suprathermal electrons aligned to the magnetic field and directed  
68 outward from the Sun. Owing to their large mean-free path, suprathermal electrons  
69 travel freely along magnetic field lines, and are therefore used as tracers of the large-scale  
70 heliospheric topology (e.g., Gosling (1990); Kahler (1987)). Although this population  
71 is usually dominated by the outward-flowing strahl, sunward-directed counter-streaming  
72 suprathermal electrons are also often recorded in the solar wind. These are observed  
73 on closed field lines with both ends attached to the Sun, such as within interplanetary  
74 coronal mass ejections (ICMEs) (e.g., Philipp (1987); Gosling et al. (1987)) or newly  
75 closed field regions due to magnetic reconnection at the heliospheric current sheet (HCS)  
76 (Gosling et al. (2006); Lavraud et al. (2009)). Counter-streaming suprathermal electrons  
77 may also occur due to the presence of magnetic field enhancements farther from the  
78 spacecraft along magnetic field lines, e.g., within CIRs, near their bounding shocks and  
79 to some distance downstream. The counterstreaming population in such cases is thought  
80 to result from wave-particle interactions and shock heating, combined with adiabatic  
81 mirroring and particle leakage into the upstream regions of the CIR (Gosling et al. (1993);

82 Steinberg et al. (2005); Skoug et al. (2006); Lavraud et al. (2010)).

83 Because of the wavy nature of the interplanetary current sheet, multiple CIRs can form  
84 in a single solar rotation. Will the presence of multiple CIRs affect the particle acceleration  
85 process? In this paper, we report, to our knowledge, the first observation of an energetic  
86 particle event associated with a CIR pair.

## 87 2. Observations

88 In this work, we use the data from STEREO’s IMPACT instrument suite  
89 (Luhmann et al. 2008). These include protons between 101.3 keV nucleon<sup>-1</sup> to 1.985  
90 MeV nucleon<sup>-1</sup> and electrons from 65 keV to 375 keV from the Solar Electron and  
91 Proton Telescope (SEPT) (Müller-Mellin et al. 2008); 4-6 MeV protons from 16 sectors  
92 of the Low Energy Telescope (LET) (Mewaldt et al. 2008); 20 keV nucleon<sup>-1</sup> to 3.6 MeV  
93 nucleon<sup>-1</sup> proton, Helium, Oxygen, and Fe ions from the Suprathermal Ion Telescope  
94 (SIT) (Mason et al. 2008b); and  $\sim 250$  eV electrons from the Solar Wind Electron  
95 Analyser (SWEA) (Sauvaud et al. 2008). We also used the Plasma and Suprathermal  
96 Ion Composition (PLASTIC) sensor (Galvin et al. 2008) for solar wind proton parameters  
97 including the speed, number density, and total pressure. The solar wind magnetic field  
98 is from the IMPACT/MAG instrument (Acuña et al. 2008). We also used data from  
99 ACE/MAG (Smith et al. 1998), ACE/SWEPAM (McComas et al. 1998), and ACE/EPAM  
100 (Gold et al 1998).

101 We define a CIR pair as two CIRs such that the end of the first CIR and the beginning  
102 of the second CIR are within 5 days. A total of 24 CIR pairs were identified in the two-year  
103 period of 2007 and 2008. The CIR pair we examine in this work occurred during Carrington  
104 Rotation (CR) 2060.

105 Figure 1 shows the trajectories (the dot-dashed curve above the equator) of the three  
 106 spacecraft (STEREO-B, ACE and STEREO-A) overplotted on the GONG PFSS magnetic  
 107 extrapolation, with open field footprints in red/green, closed field at the source surface  
 108 in blue, and heliospheric current sheet (HCS) at the source surface in black (courtesy  
 109 of NSO/GONG) for the Carrington rotation 2060. The longitudinal separation between  
 110 STEREO-A and STEREO-B was  $\sim 28^\circ$ . The solid vertical lines mark the beginning  
 111 and ending longitudes for STEREO-B. The dashed vertical lines mark the beginning and  
 112 ending longitudes for STEREO-A. ACE was located half way between STEREO-A and  
 113 STEREO-B. The coronal sources for the fast streams of the two CIRs are labeled as “C1”  
 114 and “C2” in this plot.

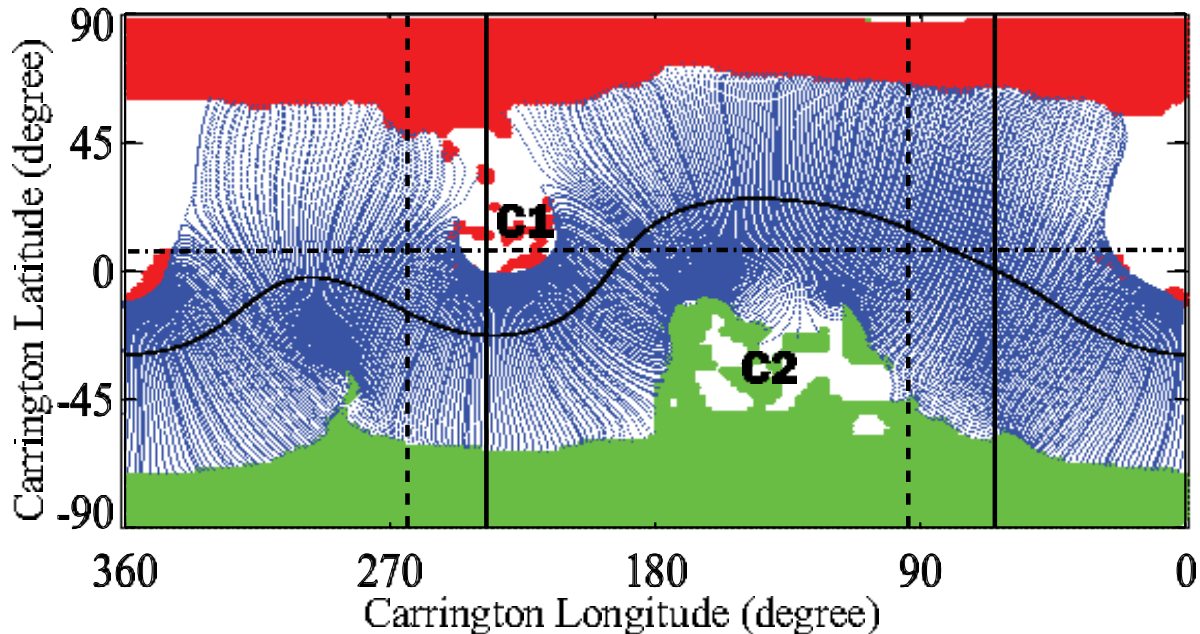


Fig. 1.— Trajectories of STEREO-A, STEREO-B and ACE, which is the horizontal line overplotted on the Gong’s synoptic map for the Carrington Rotation 2060.

115 STEREO-B *in situ* observations of the two CIRs from spacecraft are shown in Figure 2.  
 116 From top to bottom, the panels in Figure 2 are: the proton pressure, the solar wind speed,  
 117 the plasma number density, the solar wind magnetic field strength, the radial component of

118 the magnetic field, and the ratio of helium to proton fluxes at 0.320-0.452 MeV nucleon<sup>-1</sup>,  
119 0.452-0.640 MeV nucleon<sup>-1</sup> and 0.640-0.905 MeV nucleon<sup>-1</sup>.

120 As shown in Figure 2, the first CIR (hereafter CIR1) occurred from 2007 August 24  
121 (DOY 236), 14:16UT to 2007 August 26 (DOY 238), 18:10UT. The second CIR (hereafter  
122 CIR2) occurred from 2007 August 30 (DOY 242), 20:40UT to 2007 September 02 (DOY  
123 245), 00:10UT. We note that this event has been reported as event No. 14 in Table 1  
124 of Mason et al. (2009). Since there was only one peak in the ion time intensity profile,  
125 Mason et al. (2009) associated this with a single CIR. However, an examination of the solar  
126 wind profile shows that there were two CIRs. Lavraud et al. (2010) also listed them as  
127 two separate CIRs. Note that the separation angle between STEREO-A and STEREO-B  
128 at CIR mid-point at ACE for this event was 28.3° (Mason et al. 2009), so both CIRs were  
129 observed by all three spacecraft.

130 We use sudden changes in total pressure and magnetic field to identify the boundaries  
131 (so they may correspond to the shocks) of the two CIRs. These are shown as the red  
132 vertical lines in Figure 2. CIR1 had both a forward shock and a reverse shock as can be  
133 seen from the STEREO-B observations <sup>1</sup>. For CIR2, the reverse shock had completely  
134 formed at STEREO-B, but the forward shock had not.

135 The green and blue horizontal bars in the bottom three panels represent the typical  
136 ranges of helium to proton ratio found in CIRs ( $0.125 \pm 0.061$ ) and SEPs ( $0.032 \pm 0.003$ ),  
137 respectively (Mazur et al. 1993; Mason et al. 1997; Bučik et al. 2009a). These He/H ratios  
138 as well as the heavy ion ratios (not shown) clearly identify these energetic particles as being

---

<sup>1</sup>note that the online catalog maintained by L. Jian [http://www-ssc.igpp.ucla.edu/forms/stereo/stereo\\_level\\_3.html](http://www-ssc.igpp.ucla.edu/forms/stereo/stereo_level_3.html) did not list the reverse shock of CIR1 as a shock

139 from a CIR.

140 Using the CDAW Data Center catalog ([http://cdaw.gsfc.nasa.gov/CME\\_list/](http://cdaw.gsfc.nasa.gov/CME_list/)), and  
141 the Computer Aided CME Tracking (CACTus) catalog (<http://sidc.oma.be/cactus/>),  
142 as well as STEREO Level 3 data, we confirmed that the solar activity was weak between  
143 CIR1 and CIR2. During the period shown in Figure 2, there were no  $\sim >A2.0$  flares, no high  
144 frequency ( $> \text{MHz}$ ) radio bursts, nor any fast CMEs (the only detectable CME occurred  
145 on the east limb with a speed of  $162 \text{ km s}^{-1}$  on DOY 239). With these observations, any  
146 *in situ* enhancement of energetic particles is unlikely due to solar activities and must be  
147 associated with the CIRs, as is consistent with the solar wind and magnetic field signatures  
148 in Figure 2.

149 Figure 3 shows fluxes of energetic particles observed by STEREO-B during the period  
150 as shown in Figure 2. Panels 1 and 2 show the total pressure (the thermal pressure plus the  
151 magnetic field pressure) and the solar wind speed, as in Figure 2. The third panel shows the  
152 ion (mostly protons) intensities for 6 energy channels. The fourth panel shows the electron  
153 intensity for three energy channels. As in Figure 2, the boundaries of CIR1 and CIR2 are  
154 indicated by the solid vertical red lines. The stream interfaces within the two CIRs are  
155 shown as the dashed vertical magenta lines. Four 8-hour intervals between the two CIRs,  
156 labeled “A”, “B”, “C”, and “D” are also indicated. These periods will be used to examine  
157 the helium spectra and proton anisotropies (see Figure 7 below).

158 The third panel of Figure 3 shows that there were gradual but significant increases of  
159 ion fluxes in the 101.3-137.0 keV and 312.0-554.0 keV channels before the forward shock  
160 of CIR1. The intensities reached their peaks at the shock, then decayed to a plateau for  
161 a short period of time before they dropped at the beginning of day 237. The plateau  
162 feature is typical of diffusive shock acceleration and has been seen previously in CIR events  
163 (see eg. (Bučík et al. 2009a)). The drop inside CIR1 may be related to the increase in

164 solar wind speed at the same time. STEREO-B crossed the stream interface (left dashed  
165 line) several hours before DOY 238, as shown by the left dashed line. Before the reverse  
166 shock of CIR1, the intensities in the 1.1-2.0 MeV and 1.8-3.6 MeV channels showed clear  
167 gradual increases which has also been seen in other CIR events (Bučík et al. 2009a). This  
168 is possible if the reverse shock was formed inside 1 AU. Across the reverse shock, the  
169 intensities of both the 1.1-2.0 MeV and 1.8-3.6 MeV ions slowly increased. The 3.6-6.0  
170 MeV and 6.0-10.0 MeV channels also showed clear increases. Such increases contradict the  
171 scenario of diffusive shock acceleration at a single shock where one expects to see a decrease  
172 of intensity as the distance from the shock increases (see e.g. the work of Li et al. (2003,  
173 2005); Verkhoglyadova et al. (2010)).

174 The gradual increase of the ion time intensity profiles lasted until DOY 241. These  
175 increases were modulated by a transient high-speed stream on DOY 240 (marked by the  
176 vertical black line). The modulation showed no velocity dispersion and therefore could be  
177 due to connectivity issue, as discussed in Bučík et al. (2009a) for a different event. The  
178 intensity peaks for all four channels occurred at the beginning of DOY 241. Beyond DOY  
179 241, the intensities for the two highest energy channels started to decrease. Examination  
180 of Figure 2 shows that  $B_r$  reversed its sign on DOY 241. The large scale magnetic field  
181 configuration turns out to be an important key in understanding this event. Below we  
182 examine the magnetic field configuration in detail, making use of the suprathermal electron  
183 observations.

184 At the leading edge of CIR2, the four highest energy ion channels showed no increases.  
185 This is consistent with the absence of a forward shock at CIR2. Across the stream interface  
186 (between DOY 243 and 244, as indicated by the right dashed magenta line), all intensities  
187 dropped significantly. Across the reverse shock of CIR2 at the beginning of DOY 245,  
188 the intensities showed further gradual decreases, as one would expect from diffusive shock

189 acceleration in solar energetic particle events (Li et al. 2003, 2005; Verkhoglyadova et al.  
190 2010).

191 The fourth panel in Figure 3 shows electron time intensity profiles for three energy  
192 channels, 65.0-105.0 keV, 145.0-225.0 keV, and 255.0-375.0 keV. Similar to the ion  
193 observations, the most striking feature is the enhancement of intensity in between the two  
194 CIRs. Indeed, for the 65.0-105.0 channel, the peak of the time intensity profile occurred  
195 near the middle of the two CIRs; for the 145.0-225.0 keV and 255.0-375.0 keV channels,  
196 the time intensity profiles between the two CIRs are plateau-like. Such a peak and/or  
197 plateau-like feature has not been previously reported for single CIR events.

198 The time intensity profiles of ions and electrons between the two CIRs as observed  
199 by STEREO-B are very unusual for CIR events. Since the same CIR was also observed  
200 by ACE and STEREO-A, we next examine the energetic particle observations at these  
201 spacecraft.

202 Figure 4 shows the ACE observations. The top panel shows the solar wind total  
203 pressure and the second panel shows the solar wind speed. The lack of pressure at  
204 the beginning of the period is due to a data gap. The third and fourth panels are ion  
205 and electron intensities from ACE/EPAM, respectively. Comparing to the STEREO-B  
206 observations, while the 38-53 keV and 53-103 keV electrons show clear peaks, the higher  
207 energy electrons (103-175 keV) and ions did not show clear peaks. The ion intensity remains  
208 almost constant.

209 Figure 5 shows the STEREO-A observations. As in Figure 4, the top two panels display  
210 the total solar wind pressure and the solar wind speed, respectively. The third panel shows  
211 the ion (mostly proton) intensities from SEPT and proton intensities from LET, while the  
212 fourth panel shows the electron intensities from LET. Again, there were no clear peaks in  
213 the low energy ions between the two CIRs. However, for high energy ions observed by LET

214 (especially 3.6-6.0 MeV and 6.0-10.0 MeV channels), intensities gradually increased after  
 215 CIR1, until the middle of DOY 241, and then quickly dropped. Compared to ions, electrons  
 216 showed more pronounced peaks after CIR1.

217 SEP observations at ACE and STEREO-A showed similar unusual behavior, but less  
 218 prominent. This is possible if the underlying cause for the STEREO-B observation is  
 219 transient in nature and affects ACE and STEREO-A observation for a shorter period of  
 220 time. Indeed, this is an important clue for understanding this event, as discussed later.

221 We now examine how the spectrum of energetic helium ions evolved in this event.  
 222 Figure 6 shows the energetic helium spectra during the four 8-hour intervals, “A”, “B”,  
 223 “C”, and “D” shown in Figure 3. For example, at  $\sim 0.1\text{MeV/nucleon}$ , the helium intensity  
 224 during period B (C) is about twice as large as in period A. At  $\sim 2\text{MeV/nucleon}$ , the helium  
 225 intensity during periods B and C is more than 10 times larger than in period A. The  
 226 spectrum for period D is similar to the spectrum for period A, but the intensity was higher.  
 227 These spectral observations show that there are more high energy particles near the middle  
 228 of the two shocks (periods B and C) than closer to the shocks (periods A and D). Note that  
 229 period A is closer to the reverse shock of CIR1 and period D is closer to the forward shock  
 230 of CIR2.

231 The four panels in Figure 7 show sector plots of the anisotropy of 6 to 10 MeV protons  
 232 in the RT plane for the four 8-hour intervals, respectively. The Radial, Tangential, Normal  
 233 (RTN) coordinate system is used. The  $R$  direction is from the Sun to the spacecraft and  
 234 is pointing to the left; the  $T$  direction is along the  $\Omega \times \hat{R}$  direction, where  $\Omega$  is the Sun’s  
 235 spin axis; and the  $N$  direction completes the right-handed triad. The Sun is to the right in  
 236 these plots. At 1 AU, the nominal magnetic field with a Parker spiral orientation (pointing  
 237 away from the Sun) will be along the diagonal from the lower right corner to the upper left  
 238 corner (the arrow shown in panel A). We use data from the LET instrument, which has

239 a total of 16 sectors with 8 facing toward and 8 against the Sun. The convention of the  
 240 plot is such that the upper left (lower right) sector measures ions coming from the upper  
 241 left (lower right). The lengths of the sectors denote the intensities of the fluxes as seen by  
 242 that detector with the scale shown in the  $x$  and  $y$ -axis. The red and blue lines shown in the  
 243 panel represent the 2-minute averaged magnetic field directions, with red (blue) indicating  
 244 negative  $B_r$  and blue positive  $B_r$ .

245 In panel A, except for two intervals, the magnetic field points toward the Sun and  
 246 clustered around the Parker spiral direction, but with a large spread. The proton flux was  
 247 lower than those in the other three panels. The flux was rather isotropic, with slightly more  
 248 particles coming into the 8 upper-left detectors than coming into the 8 lower-right detectors.

249 In panel B, the directions of the magnetic field still points toward the Sun. The spread  
 250 of the magnetic field direction is narrower than in panel A and the center of the distribution  
 251 is slightly inclined towards the R direction. The flux is more than 10 times higher than  
 252 those in Panel A and there is a clear anisotropy in that more protons are propagating  
 253 towards the Sun than away. The anisotropy suggests that the source of the 4-6 MeV protons  
 254 was located outside 1 AU. These protons were presumably accelerated at the reverse shock  
 255 of CIR1 (now beyond 1 AU) and propagated back to 1 AU. Note that the fluxes detected by  
 256 the 8 detectors facing against the Sun (the upper left 8 sectors) do not differ much between  
 257 themselves,  $\sim 0.012/(\text{cm}^2 \text{ s sr MeV/n})$ . Similarly the fluxes detected by the 8 detectors  
 258 facing the Sun (the lower right 8 sectors) did not differ much,  $\sim 0.007/(\text{cm}^2 \text{ s sr MeV/n})$ .  
 259 So the fluxes are isotropic in each hemispheres. Note that particles propagating towards  
 260 the Sun can be reflected, and then as they move back away from the Sun, their pitch angles  
 261 will approach zero due to the “magnetic focusing” effect. However, the fact that the pitch  
 262 angle distributions (PADs) were isotropic within each hemisphere suggests that pitch angle  
 263 diffusion dominated over magnetic focusing. As a measure of the anisotropy, we find the

264 ratio of the sunward to anti-sunward fluxes is  $\sim 2$ . This value depends very much on the  
265 pitch angle diffusion coefficient and can be used to constrain models of particle acceleration  
266 and transport in CIRs.

267 Panel C is for the period where the peak of the 6-10 MeV proton intensity occurred.  
268 The magnetic field showed a clear bi-polar distribution during this period: when  $B_r < 0$   
269 (the red lines), the magnetic fields were generally aligned with the nominal Parker spiral  
270 direction; when  $B_r > 0$  (the blue lines), the magnetic fields were aligned mostly between the  
271 radial direction and that is perpendicular to the nominal Parker spiral direction. Compared  
272 to panel B, the proton flux was enhanced. The pitch angle distribution was almost isotropic,  
273 with slightly more particles propagating away from the Sun.

274 The period shown in panel D was closer to CIR2. During this period  $B_r > 0$ , so the  
275 magnetic field was pointing away from the Sun. Period D was thus on the opposite side of  
276 the HCS. The proton flux was typically smaller than in periods B and C (note the scales  
277 in panel A and D are different from those in panels B and C), but higher than those in  
278 period A. There was a significant anisotropy in the angular distribution, with more protons  
279 propagating away from the Sun.

280 The observations of energetic ions and electrons described above are very unusual and  
281 were never reported in individual CIR events. For example, in typical single CIRs the  
282 maximum intensities occur near either the forward or the reverse shock, and after spacecraft  
283 passage through the reverse shock, the intensities usually drop quickly. Furthermore the  
284 anisotropy of SEPs after the reverse shock is usually sunward.

### 3. Discussion

285

286 What caused all these unusual observations in this event? The presence of the second  
 287 CIR likely plays an important role. However these observations are also rare for CIR pairs.  
 288 Indeed as we will discuss in the following, for the Carrington Rotation immediately before  
 289 and after CR2060, where CIR pairs also appeared, energetic ion intensity observations  
 290 showed the normal temporal behavior of single CIR cases. This is somewhat expected  
 291 because unless the two CIRs are magnetically connected, the presence of a second CIR will  
 292 have no effects on the energetic particles associated with the first CIR, and vice versa.

293 The above argument suggests that magnetic connection is important in the case of  
 294 CR2060. We argue in the following that these observations (as shown in Figures 3 to 7)  
 295 resulted from particle acceleration and trapping between the reverse shock of the first CIR  
 296 and the forward shock of the second CIR through a large scale “U-shape” magnetic field  
 297 that connects these two shocks. We illustrated schematically in Figure 8. The U-shaped  
 298 magnetic field was possibly caused by reconnection that occurred high in the corona.  
 299 Previously, Luhmann et al. (1998) and Li et al. (1998) suggested that such reconnections  
 300 may constantly occur near the cusp of the helmet streamers due to the continuous global  
 301 evolution of coronal fields. In a numerical modeling effort, Chen et al. (2009) noted that  
 302 reconnections can take place above a streamer cusp repeatedly as a result of insufficient  
 303 magnetic confinement of streamer plasmas.

304 In Figure 8, the dashed semicircle is the approximate spacecraft trajectory with respect  
 305 to the Sun in the co-rotating frame. The spacecraft moves along the semicircle in the  
 306 clockwise direction (as shown by the arrow). The labels A, B, C, D correspond to the 4  
 307 periods shown in Figure 3. The two compression regions are indicated by the horizontal  
 308 and inclined lines. The stream interfaces are shown as the dashed lines inside the two  
 309 compression regions. The solid lines in red and blue and with arrowheads are the magnetic

310 field lines. Red denotes a negative  $B_r$  and blue denotes a positive  $B_r$ . The four dark black  
 311 lines are the four shocks. The forward shocks are formed in the slow wind and the reverse  
 312 shocks are formed in the fast wind. The forward and reverse shocks bounded the CIRs.  
 313 Note that as drawn in Figure 8, both the forward and reverse shocks of CIR1 are formed  
 314 inside 1 AU. In comparison, the forward shock of CIR2 is formed outside 1 AU, but the  
 315 reverse shock is formed inside 1 AU, as required by the *in situ* observations as shown in  
 316 Figure 2. Three U-shaped magnetic field lines are shown in Figure 8. These are drawn  
 317 to help understanding the time intensity profiles shown in Figure 3 and the anisotropy  
 318 observations shown in Figure 7.

319 Referring to features in Figure 8, we now describe a scenario to explain the STEREO-B  
 320 observations. Consider first period A, at this time STB had just passed the newly developed  
 321 reverse shock from left (downstream) to right (upstream). It was close to the shock, so  
 322 the distribution of the energetic particles did not show a strong anisotropy. Furthermore,  
 323 since the shock was newly formed at this distance, the acceleration was less efficient and  
 324 the intensity of the energetic particles was low. As STB moved clockwise to period B, it  
 325 connected to the part of the shock that was further away, where the shock was stronger.  
 326 Since the shock was the source of the energetic particles, we expect to see most energetic  
 327 particles propagating sunward during this period, as observed in Figure 7. Although most  
 328 particles were flowing toward the Sun,  $\sim 1/3$  were moving away from the Sun. This is  
 329 not unusual in CIR events where the pitch angle anisotropies are usually modest. A small  
 330 anisotropy is likely due to a strong pitch angle scattering. Furthermore magnetic reflection  
 331 of sunward flowing particles, as they move closer to the Sun, can reverse their propagation  
 332 directions. So even if pitch angle scattering is not strong, these reflected particles will be  
 333 observed as moving away from the Sun.

334 Moving from period A to B, the particle intensity increases, and the anisotropy also

335 increases. In the U-shaped magnetic field scenario, this is due to the spacecraft being  
 336 connected to stronger sources (further away). As the spacecraft further moved to period C,  
 337 we find that the direction of the magnetic field went through a phase during which it was  
 338 mostly perpendicular to the nominal Parker field direction and eventually the  $B_r$  flipped  
 339 sign. This can be explained naturally with the U-shaped magnetic field, since in this case,  
 340 the B field direction had to undergo a change from a Parker-spiral-like with  $B_r < 0$  to an  
 341 intermediate state where  $B_r = 0$  and finally to a direction with  $B_r > 0$ . During period C,  
 342 the intensity of energetic ions also increases. This is not surprising since now the U-shaped  
 343 field lines connected to both the reverse shock of CIR1 and the forward shock of CIR2,  
 344 so that accelerated particles are effectively trapped between the two shocks. Furthermore,  
 345 since it was in the middle of CIR1 and CIR2, it connected to the furthest and strongest  
 346 parts of both shocks, consequently the acceleration was the most efficient. Also note that  
 347 further away the shock compression ratio could be larger and the particle spectrum can be  
 348 therefore harder. That particles are now trapped between two shocks also implies that the  
 349 anisotropy in period C will be smaller than that in period B. This is what the observations  
 350 show in Figure 7. We note that for energetic electrons, because they move fast, they may  
 351 undergo multiple reflections between the reverse shock of CIR1 and the forward shock of  
 352 CIR2. This may lead to a more efficient acceleration than that at a single shock.

353 In period D, the U-shaped field lines were still connected to the reverse shock of CIR1,  
 354 but not connected to the forward shock of CIR2 because it was not yet formed at 1 AU  
 355 (during period D the field lines are the same as those in period A and B). The U-shaped  
 356 magnetic field is not connected to the forward shock of the CIR2, so only limited reflection  
 357 can occur locally in CIR2, and therefore the energetic particles in period D were mostly  
 358 streaming away from the Sun. This agrees with the anisotropy observations in Figure 7.  
 359 Furthermore, the absence of the reflection also implies that the intensity of energetic ions  
 360 in period D will drop comparing to period C. This agrees with the time-intensity profile

361 observations shown in Figure 3 and Figure 7. Note that the intensity in period D is  
362 comparable to those in period A and B. Also we remark that magnetic field enhancement  
363 in a CIR without shock can also reflect particles, but presumably of less efficiency than if  
364 there is a shock.

365 In our proposed scenario, the large scale U-shaped magnetic field topology is the  
366 key. So it is important to see if there is corroborating observational evidence for this. As  
367 explained in the introduction, solar wind suprathermal electrons can be used to infer the  
368 large-scale topology of the interplanetary magnetic field (e.g., Gosling (1990); Kahler  
369 (1987)). Recent studies (Steinberg et al. 2005; Skoug et al. 2006; Lavraud et al. 2010)  
370 showed that counter-streaming suprathermal electrons are frequently observed in the  
371 vicinity of CIRs, owing to wave-particle interactions and shock heating, combined with  
372 adiabatic mirroring and particle leakage into the upstream regions (both into the adjacent  
373 slow and fast winds).

374 However, statistical analyses (Lavraud et al. 2010) showed that such counter-streaming  
375 features are only observed to some limited distance downstream of the CIR bounding  
376 shocks/compressions. In other words, they are not expected to extend all the way from one  
377 CIR to the next. We thus now examine the pitch angle distributions (PAD) of  $\sim 250$  eV  
378 electrons in the context of the proposed U-shaped topology. We first consider STEREO-B  
379 observations. In Figure 9, the top panel displays the normalized (for each sample)  
380 electron PAD, the second panel shows the solar wind speed, and the next four panels  
381 show the magnetic field components and its magnitude. This figure shows a dominant  
382 anti-field-aligned strahl until DOY  $\sim 239$ .

383 On day 236, we note a short duration reversal of the dominant PAD polarity. However,  
384 this is commonly observed when strong acceleration and reflection of suprathermal electrons  
385 occurs at CIR shocks (cf. (Steinberg et al. 2005; Skoug et al. 2006)). Although not

386 shown, the fluxes of the  $180^\circ$  population actually remained the same as adjacent regions  
 387 during this short interval, but the overwhelming fluxes of the reflected population make the  
 388 normalized PADs appear dominated by this reflected population.

389 The most important PAD feature is seen between the two CIRs. Starting slightly before  
 390 DOY 379 at the time of the reverse shock of CIR1, and lasting until the beginning of CIR2  
 391 (DOY 243), STEREO-B recorded unusual and essentially continuous counter-streaming  
 392 PADs. As shown in previous studies, this feature is not necessarily related to a closed field  
 393 topology. It is often seen upstream of CIR shocks, but again what makes it unusual here  
 394 is that it is observed continuously between the two CIRs. In the proposed scenario of a  
 395 U-shaped magnetic topology connecting the reverse shock of CIR1 and the forward shock  
 396 of CIR2, counter-streaming suprathermal electrons is a natural consequence; for the same  
 397 reasons as explained previously for more energetic ions and electrons. A U-shaped magnetic  
 398 topology also implies that  $B_r$  will reverse sign, as indicated by the red vertical line in Figure  
 399 9. Note that the  $B_r$  reversal is in any case expected between two consecutive CIRs, if these  
 400 do not come from pseudo streamers, as is the case here.

401 Figure 10 and Figure 11 are similar to Figure 9, but for ACE and STEREO-A,  
 402 respectively. Compared to STEREO-B, the counter-streaming features at ACE and  
 403 STEREO-A are much less prominent, and of shorter durations. The vertical red lines  
 404 mark the times when  $B_r$  changes sign at ACE and STEREO-A. In both cases,  $B_r$  reversed  
 405 sign in the slow solar wind and close to CIR2, as is usually the case. This is unlike the  
 406  $B_r$  sign change at STEREO-B which is very significantly farther from CIR2. We take  
 407 these observations as additional arguments in favor of a large-scale U-shaped topology, as  
 408 depicted in Figure 8, which is caused by magnetic reconnection in the high corona. This  
 409 phenomenon is transient in nature since ACE and STEREO-A measurements do not show  
 410 the same continuous PAD properties as STEREO-B.

411 As discussed next, these properties are also not found for the previous and next  
412 Carrington rotations.

### 413 **3.1. Energetic particle observations from the preceding and the following** 414 **Carrington Rotations**

415 The observations discussed so far have motivated us to conjecture the existence of a  
416 large scale U-shaped magnetic field topology between the reverse shock of CIR1 and the  
417 forward shock of CIR2. The U-shaped magnetic field was possibly caused by reconnection  
418 that occurred high in the corona. As such, it is expected to be transient in nature, which  
419 explains why these unusual energetic particle observations were most prominent at one  
420 spacecraft, in this case STEREO-B. Such a transient nature of the U-shaped magnetic field  
421 also implies that similar observations are not expected to emerge for the CIR pairs before  
422 and after CR2060. We now examine the energetic particle observations from the CIRs  
423 in the preceding and following Carrington Rotations by STEREO-B. These are shown in  
424 Figure 12 and Figure 13.

425 For CR2059, while the two high speed solar wind streams are evident, the shock pair  
426 that bounded the first CIR could not be identified. In comparison, the forward shock, but  
427 not the reverse shock, of the second CIR has developed at 1 AU. There was clear signatures  
428 of particle acceleration at the second CIR as shown by the enhancement of electrons and  
429 ions in most of the energy channels. The intensities of the 65 to 105 keV electron and  
430 101.3 to 137.0 keV/nucleon ion showed noticeable enhancement at the first CIR. The time  
431 intensity profiles between the two CIRs showed a very regular behavior as expected since  
432 there was no reverse shock associated with the first CIR.

433 For the CR2061, the shock pairs that bounded both CIRs can be clearly seen, making

434 it a good comparison to CR2060. Compared to Figure 3, we see stark differences in the  
435 time intensity profiles between the CIR pairs. In CR2061, there were the normal drop-outs  
436 followed by gradual enhancements of energetic electrons and ions between the two CIRs.  
437 This is best illustrated by the 1.8-3.6 MeV ion channel. Without the U-shaped magnetic  
438 field topology, this drop-out is a normal behavior since the spacecraft moved further away  
439 from the reverse shock of the first CIR. Similarly the subsequent gradual increase is due to  
440 the spacecraft becoming closer to the forward shock of the second CIR.

441 So the presence of a CIR pair is only a necessary condition for the observations shown  
442 in Figure 3. In our proposed scenario, the essential requirement for the unusual intensity  
443 enhancements between the two CIRs is a field that connects the two CIRs (to be more  
444 specific, the reverse shock of the first CIR and the forward shock of the second CIR). This  
445 is achieved through magnetic reconnection in the high corona.

#### 446 4. Conclusion

447 We report the observation of the acceleration and trapping of energetic ions and  
448 electrons at a CIR pair. The event occurred in Carrington Rotation (CR) 2060 and the two  
449 CIRs, with a separation less than 5 days, were observed by three spacecraft: STEREO-B,  
450 ACE and STEREO-A.

451 Several distinct observational features in this CIR-pair event made this event very  
452 unusual. These features are:

453 1) The time intensity profiles of high energy ions and electrons show a peak between  
454 the two CIRs.

455 2) The magnetic field changed sign in between the CIR-pair, in a fashion consistent  
456 with regular CIRs, rather than CIRs from a pseudostreamer.

457 3) The PAD of high energy protons between the two CIRs showed an unusual sequence  
458 of first being nearly isotropic, followed by mostly sunward propagating, then isotropic, and  
459 finally mostly anti-sunward propagating.

460 4) The energetic helium spectra were harder in between the two CIRs than near the  
461 CIR shocks.

462 5) Counter-streaming suprathermal electrons were observed continuously between  
463 CIR1 and CIR2.

464 These features have motivated us to propose a U-shaped large-scale magnetic field  
465 topology connecting the reverse shock of the first CIR and the forward shock of the second  
466 CIR. A U-shaped magnetic field can simultaneously explain all the above observations.  
467 The key point is that a magnetic field connecting the two shocks (the reverse shock of  
468 CIR1 and the forward shock of CIR2) will allow particles to be trapped and accelerated  
469 between the two shocks. We conjecture that magnetic reconnection occurring in the high  
470 corona is the cause of such a U-shaped magnetic field. After reconnection, the U-shaped  
471 magnetic field propagates out to the heliosphere. We infer that the magnetic reconnection  
472 process is transient in structure because observations from ACE and STEREO-A for the  
473 same event were less prominent and because there were no similar observations during  
474 the preceding and following Carrington rotations. In a future paper, we plan to examine  
475 particle acceleration at a CIR-pair with a U-shaped magnetic field configuration using a  
476 test particle simulation.

477 This work is supported in part by NSF grants AGS1135432 and ATM0847719, and  
478 NASA grant NNX13AE07G at UAH, NNSFC41331068, 41274175, 41028004, and NSBRSF  
479 2012CB825601 at SDUWH, NNSFC Y2503BA110 at NSSC, NSF grant AGS-0962653 and  
480 contract SA4889-26309 from the University of California Berkeley at APL, and NSF grant

<sup>481</sup> AGS-0962666 at SWRI. We thank the referee for very useful suggestions.

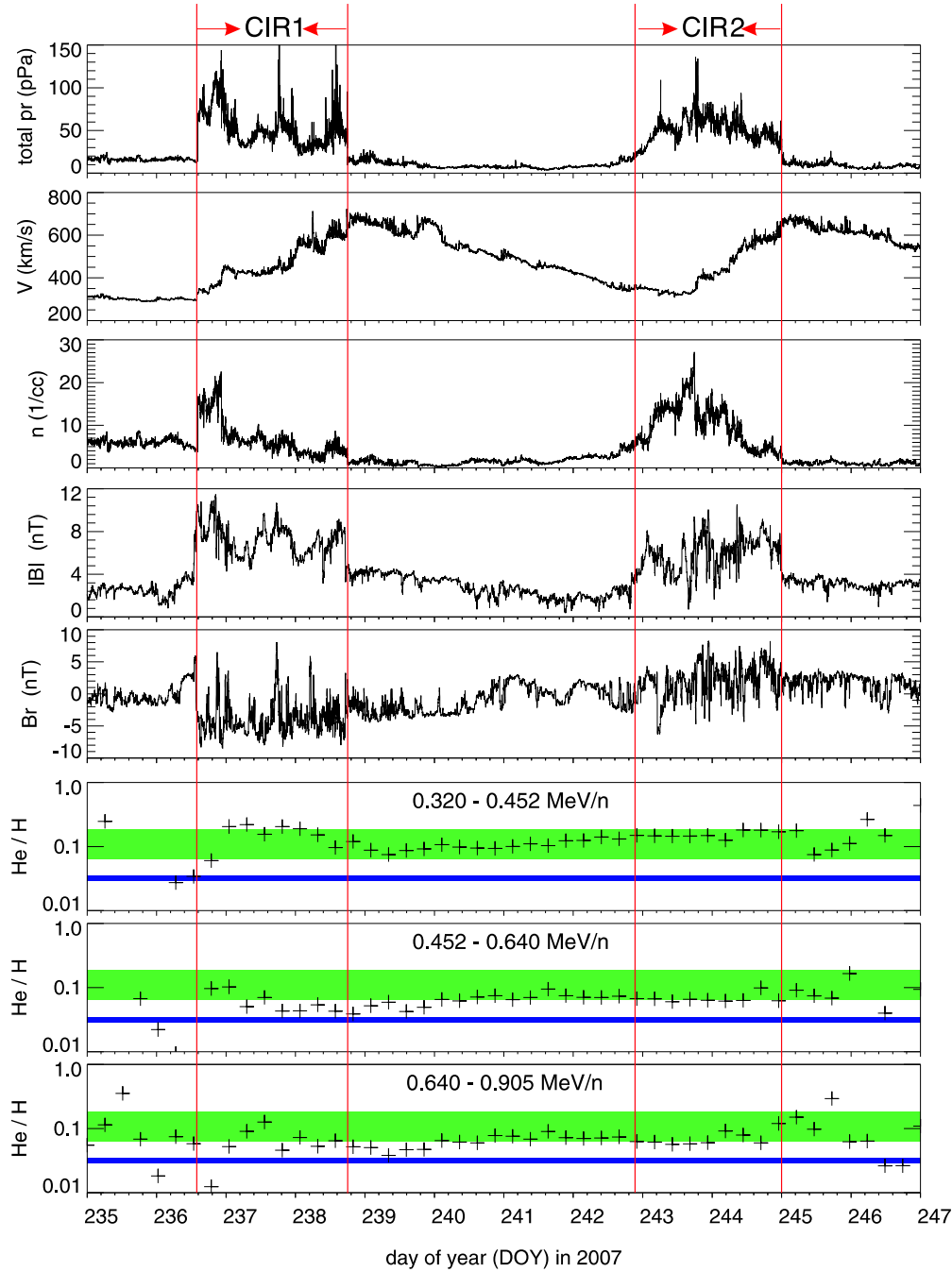


Fig. 2.— STEREO-B observations showing from top to bottom: plasma total pressure, solar wind speed, total magnetic field strength, radial magnetic field component, plasma number density, and the ratio of helium to proton at 0.320-0.452 MeV nucleon<sup>-1</sup>, 0.452-0.640 MeV nucleon<sup>-1</sup> and 0.640-0.905 MeV nucleon<sup>-1</sup> are shown.

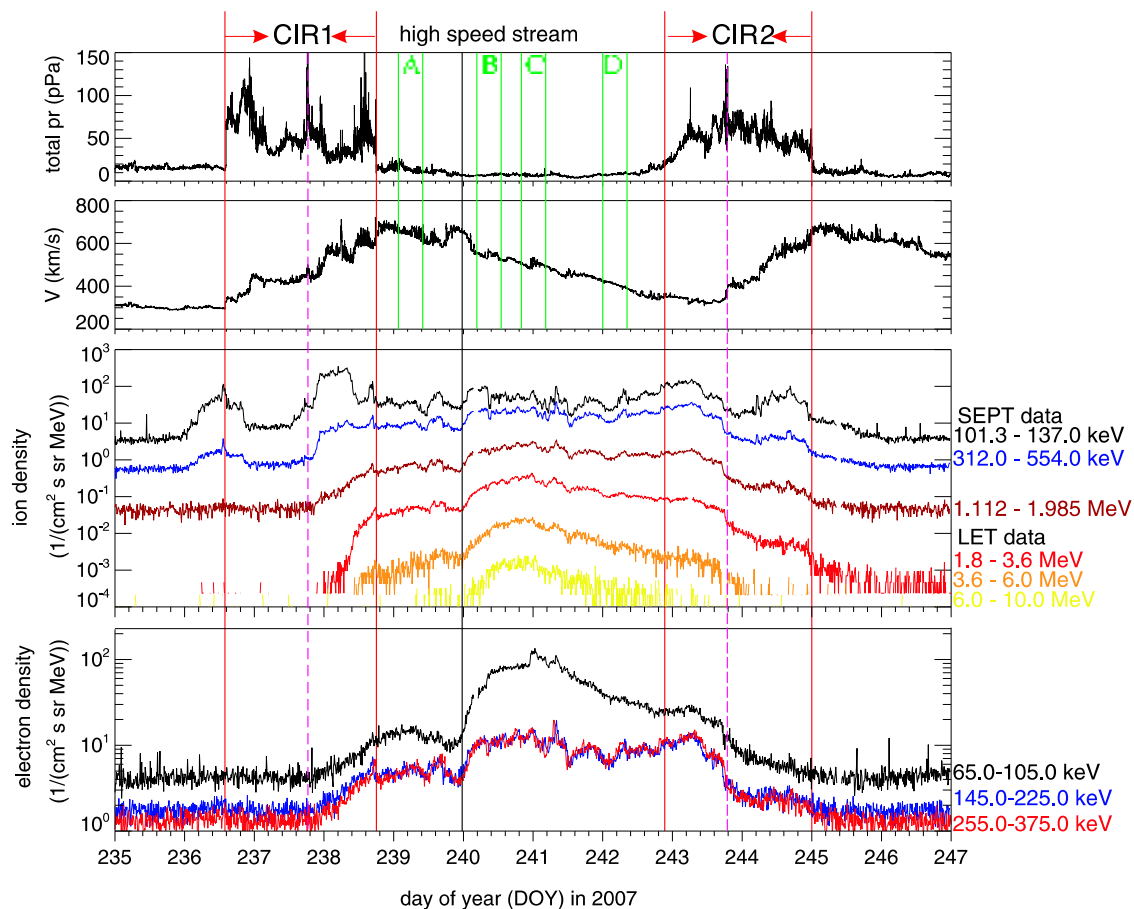


Fig. 3.— STEREO-B observations of energetic electrons and ions of the CIR-pair event. From top to bottom: solar wind total pressure, solar wind speed, ion and electron time intensity profiles from IMPACT/SEP. The four red vertical lines are the boundaries of the two CIRs and the two dashed vertical lines are the stream-interface of the two CIRs. The black vertical line marks the occurrence of a transient high-speed stream that occurred on DOY 240.

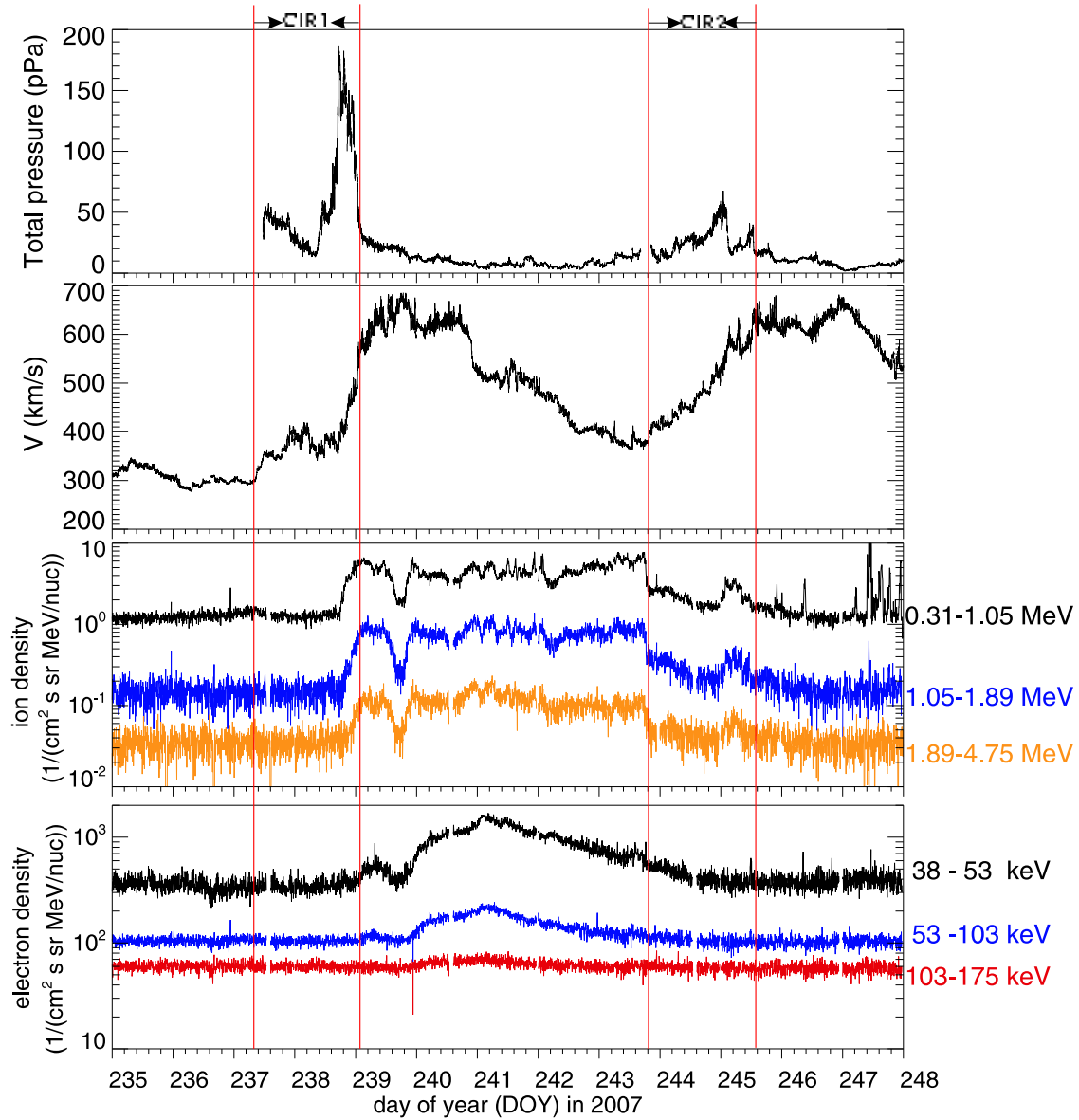


Fig. 4.— ACE observations of energetic electrons and ions of the CIR-pair event. From top to bottom: solar wind total pressure, solar wind speed, time intensity profiles for ions (mostly protons) and electrons from ACE/EPAM. The four vertical lines mark the boundaries of the two CIRs.

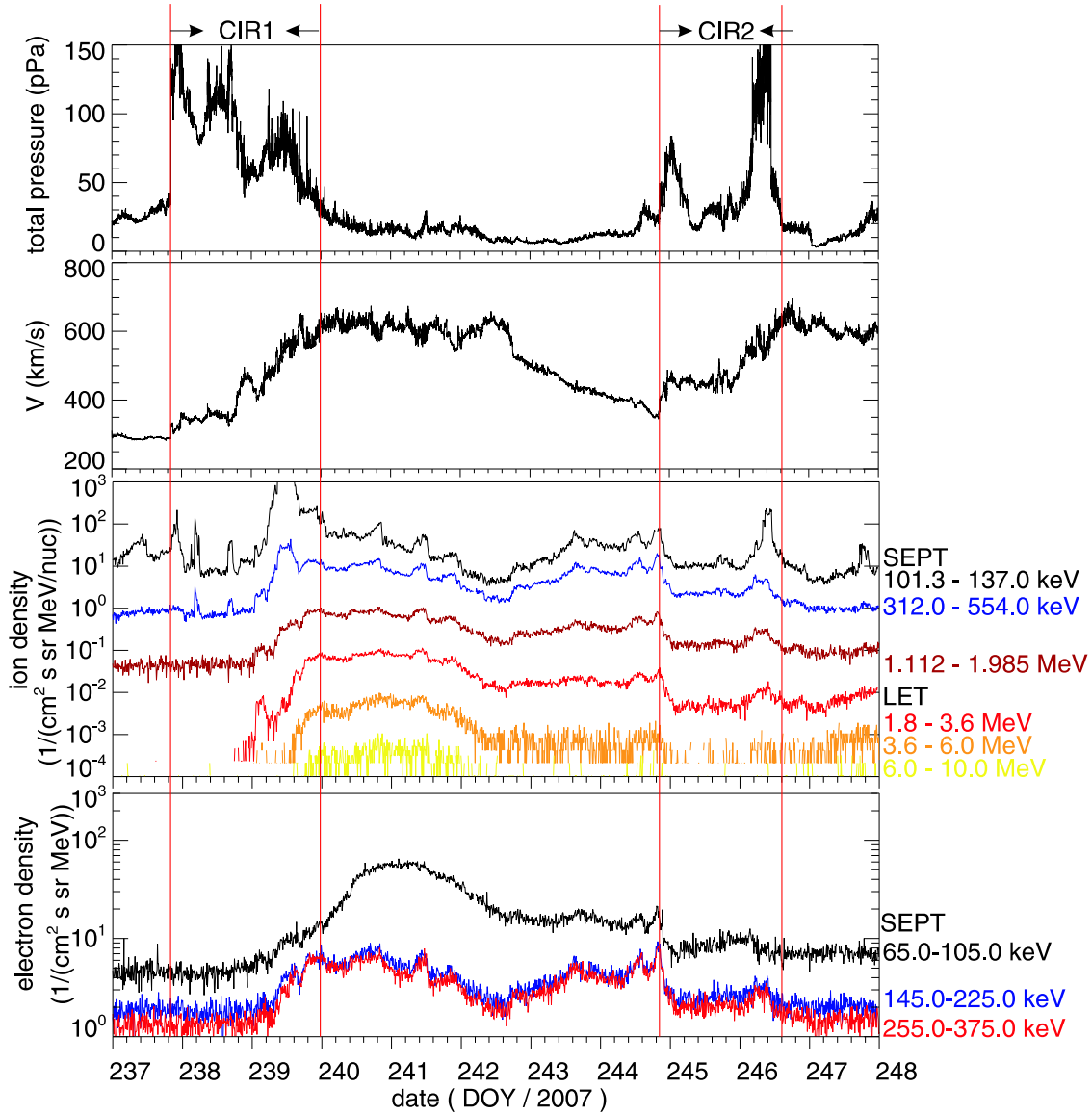


Fig. 5.— STEREO-A observations for the CIR-pair event. From top to bottom: solar wind total pressure, solar wind speed, time intensity profiles from IMPACT/SEP ion and electron measurements. The four solid vertical lines are the boundaries of the two CIRs.

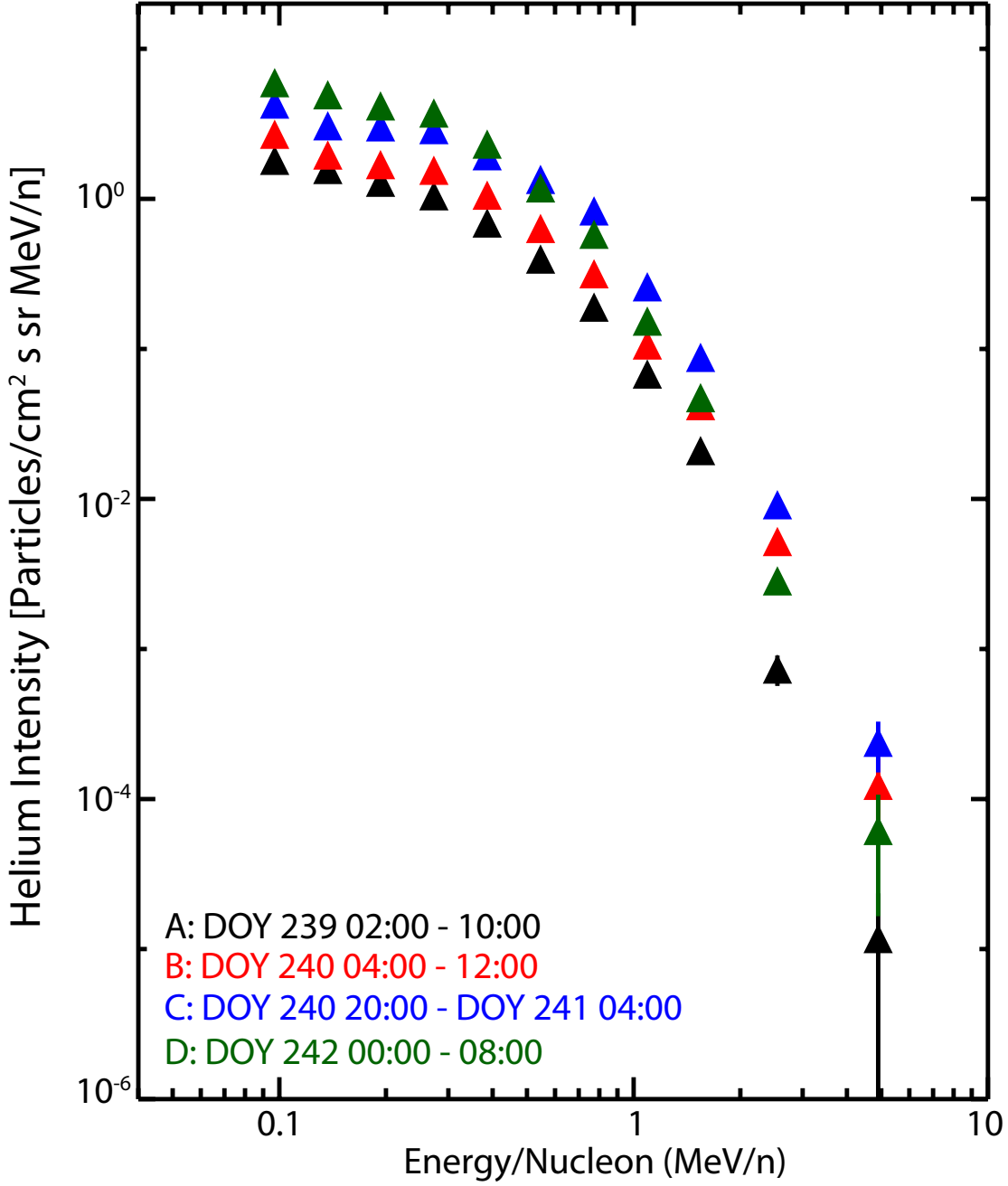


Fig. 6.— The spectra of energetic helium in the four periods: “A”, “B”, “C”, and “D” shown in Figure 3.

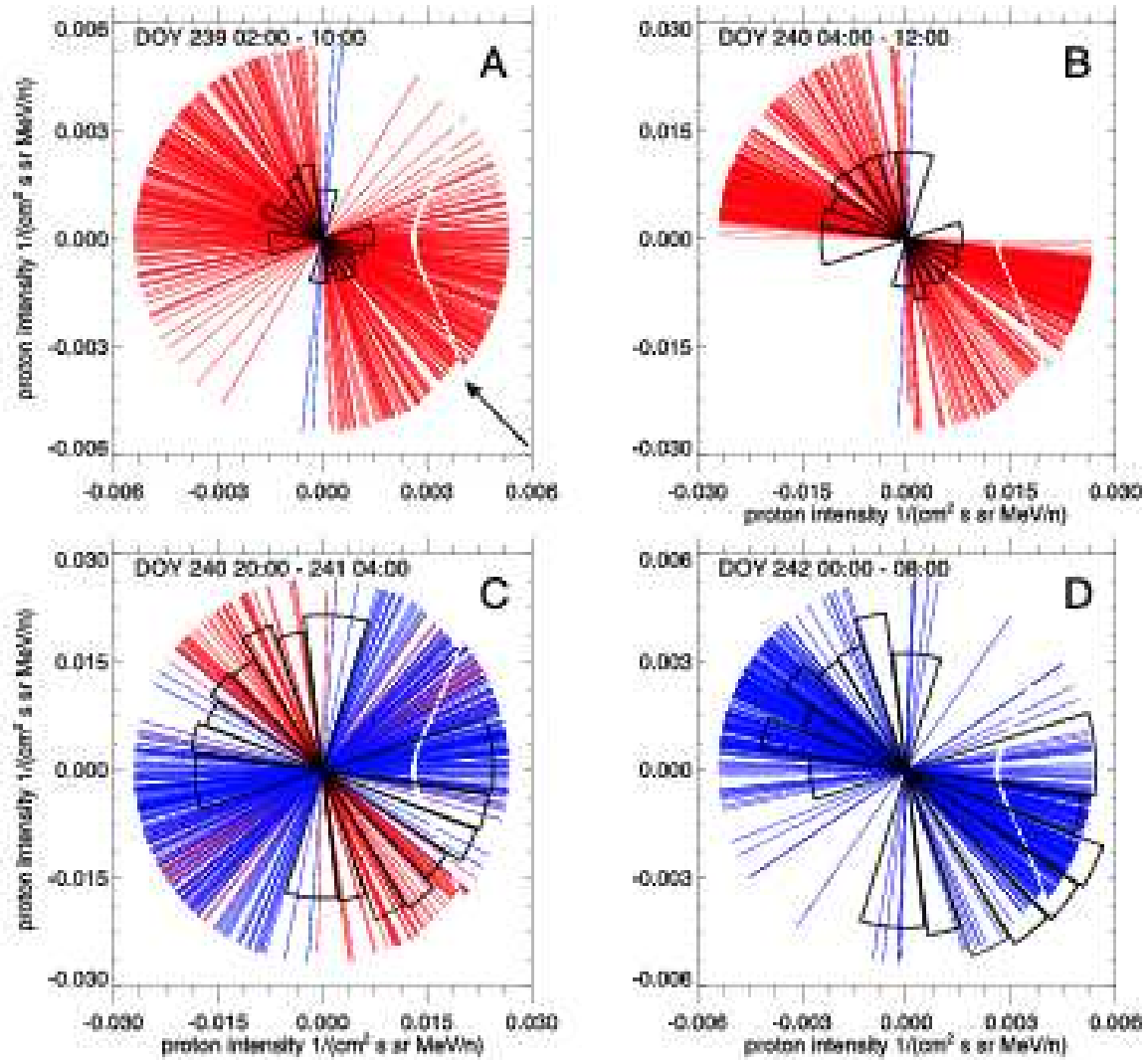


Fig. 7.— The anisotropy plots of 6-10 MeV protons from the STEREO-B LET instrument during the intervals A-D in Figure 3. The four panels are the sector plots of protons; note different intensity scales for the panels. The RTN coordinate system is used. The Sun is to the right. The length of the sectors represent the intensity of protons in the 16 sectors, respectively. Red and blue lines show 1 minute average IMF directions, with red indicating negative  $B_r$ , blue indicating positive  $B_r$ .

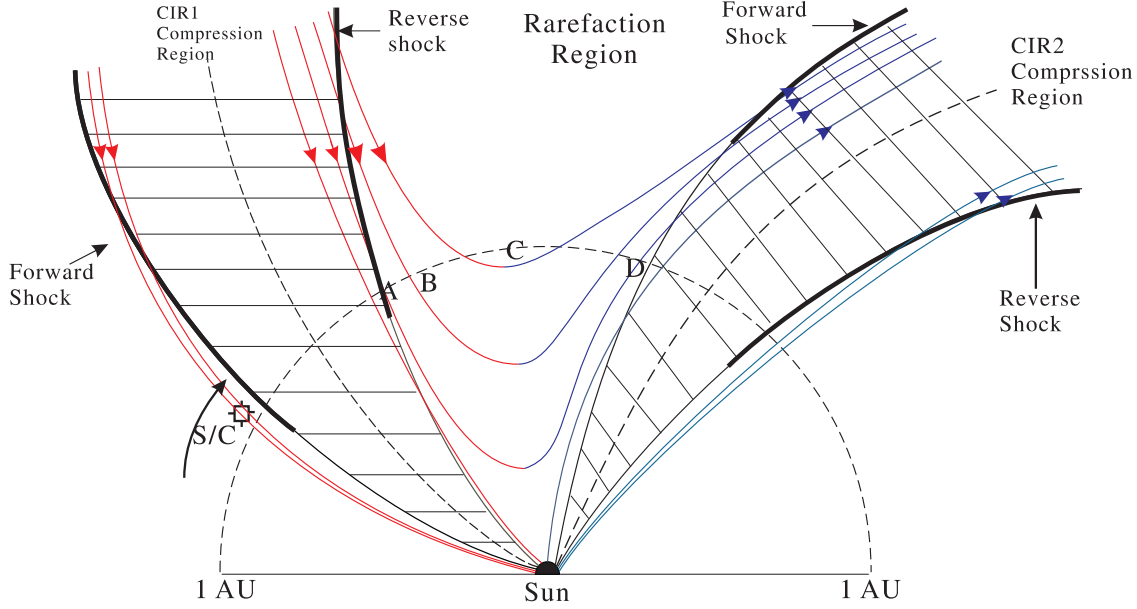


Fig. 8.— Cartoon showing the configuration of the magnetic field in the CIR-pair event. We conjecture that the U-shaped magnetic field is due to magnetic reconnection that occurred at high corona. The color shows the sense of the magnetic field: red is negative (arrows pointing to the Sun) and blue is positive (arrows pointing away from the Sun). The spacecraft trajectory, as seen from the co-rotating frame, is clockwise along the semi-circle. The two shaded areas are the compression regions. The region between the two CIRs is the rarefaction region. The forward and the reverse shocks are shown as the dark black curves. Note that as shown in the cartoon, the forward shock and the reverse shock of CIR1 and the reverse shock of CIR2 are formed inside 1 AU, while the forward shock of CIR2 is formed outside 1 AU. The U-shaped magnetic field line is proposed to account for the observations of both the reversal of the magnetic field sense and the anisotropy observations of energetic particles between the two CIRs.

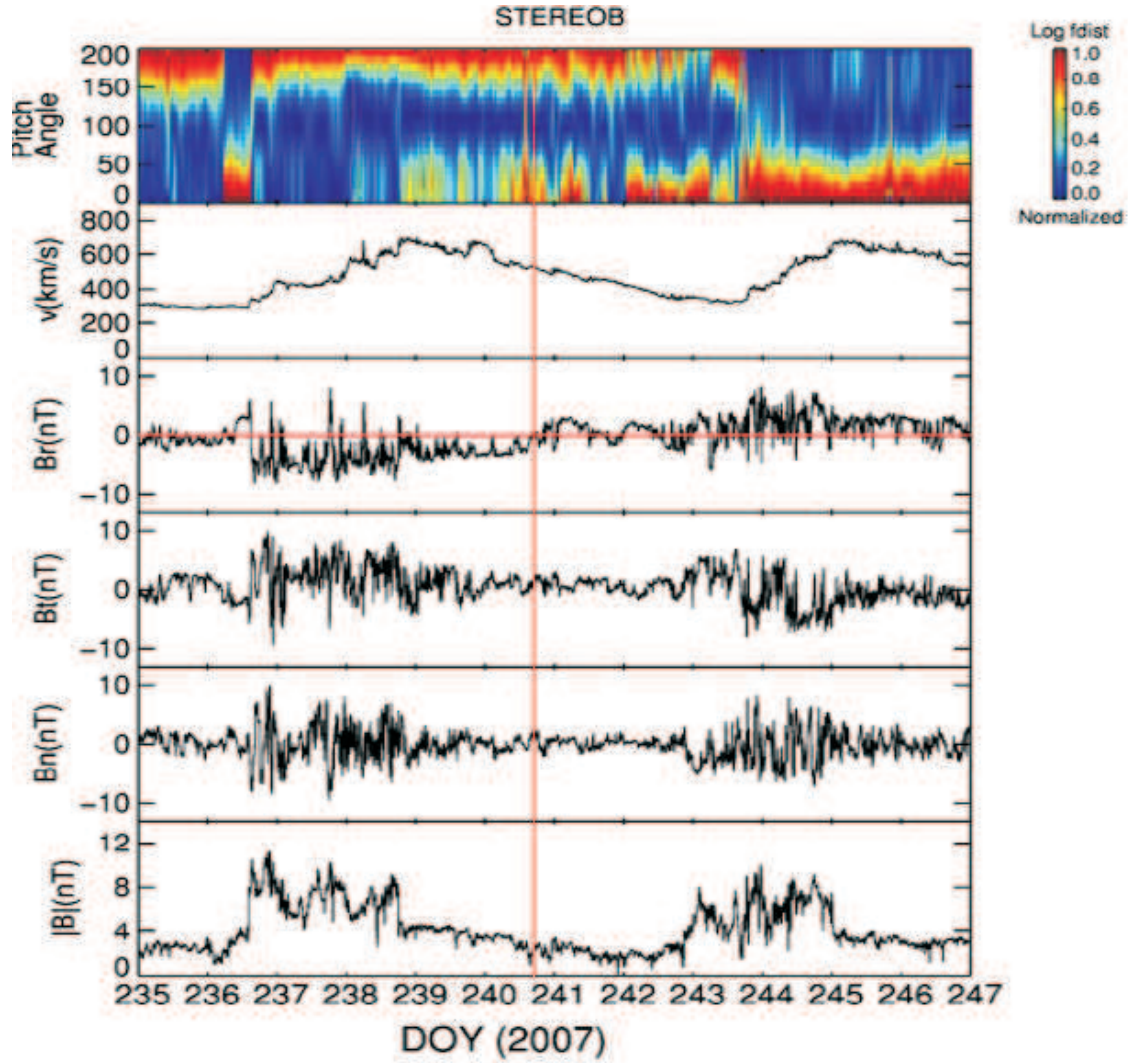


Fig. 9.— STEREO-B observations from top to bottom: the PAD of 246.62 eV strahl electrons; solar wind proton speed;  $R$ ,  $T$ , and  $N$  components of the vector magnetic field; and total magnetic field magnitude. The reversal of  $B_r$  is indicated by the vertical red line.

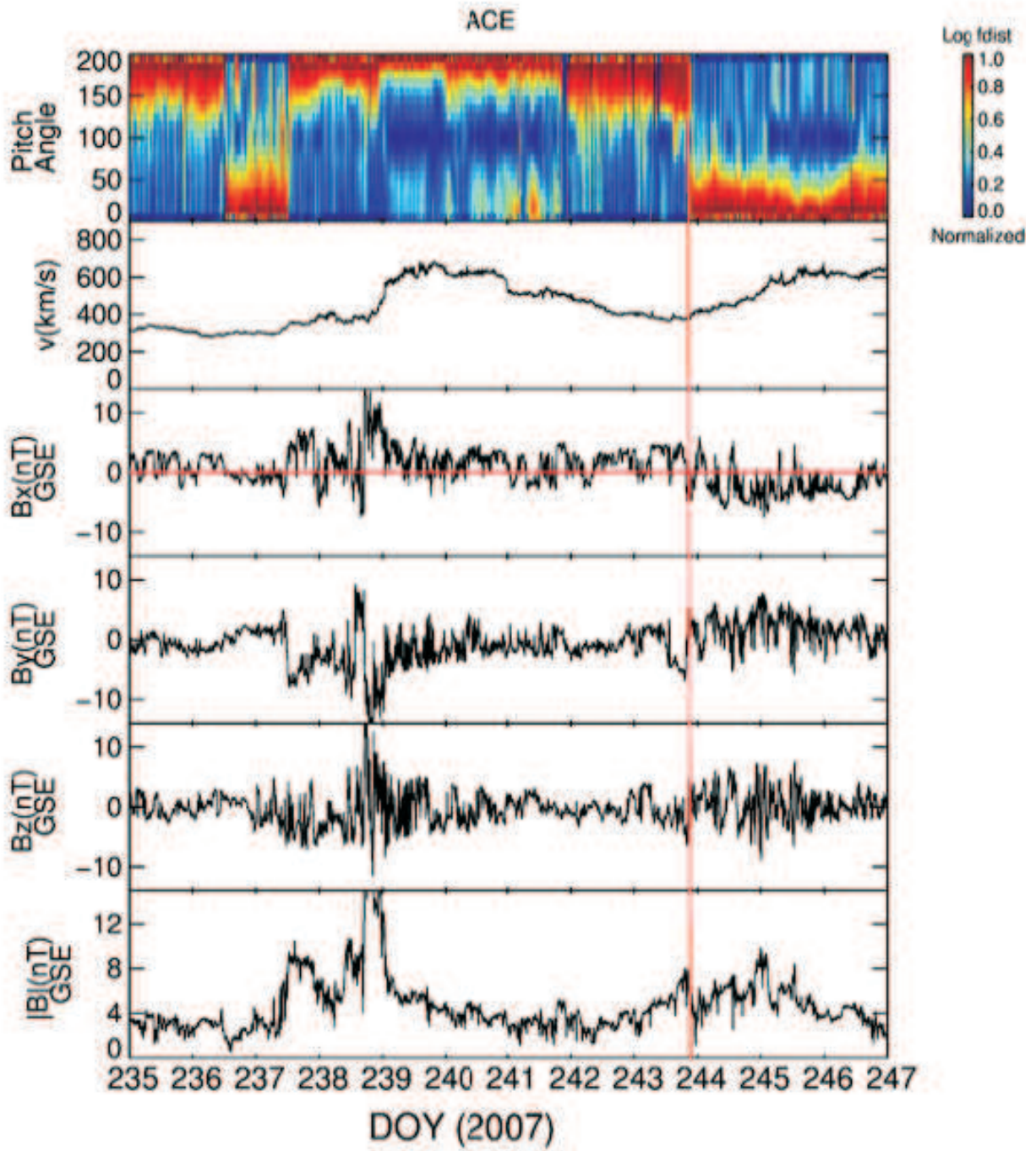


Fig. 10.— Similar to figure 9, but for ACE. Note that the ACE observation uses the GSE coordinate system, while STEREO-A and B use the RTN system. The reversal of  $B_r$  is indicated by the vertical red line.

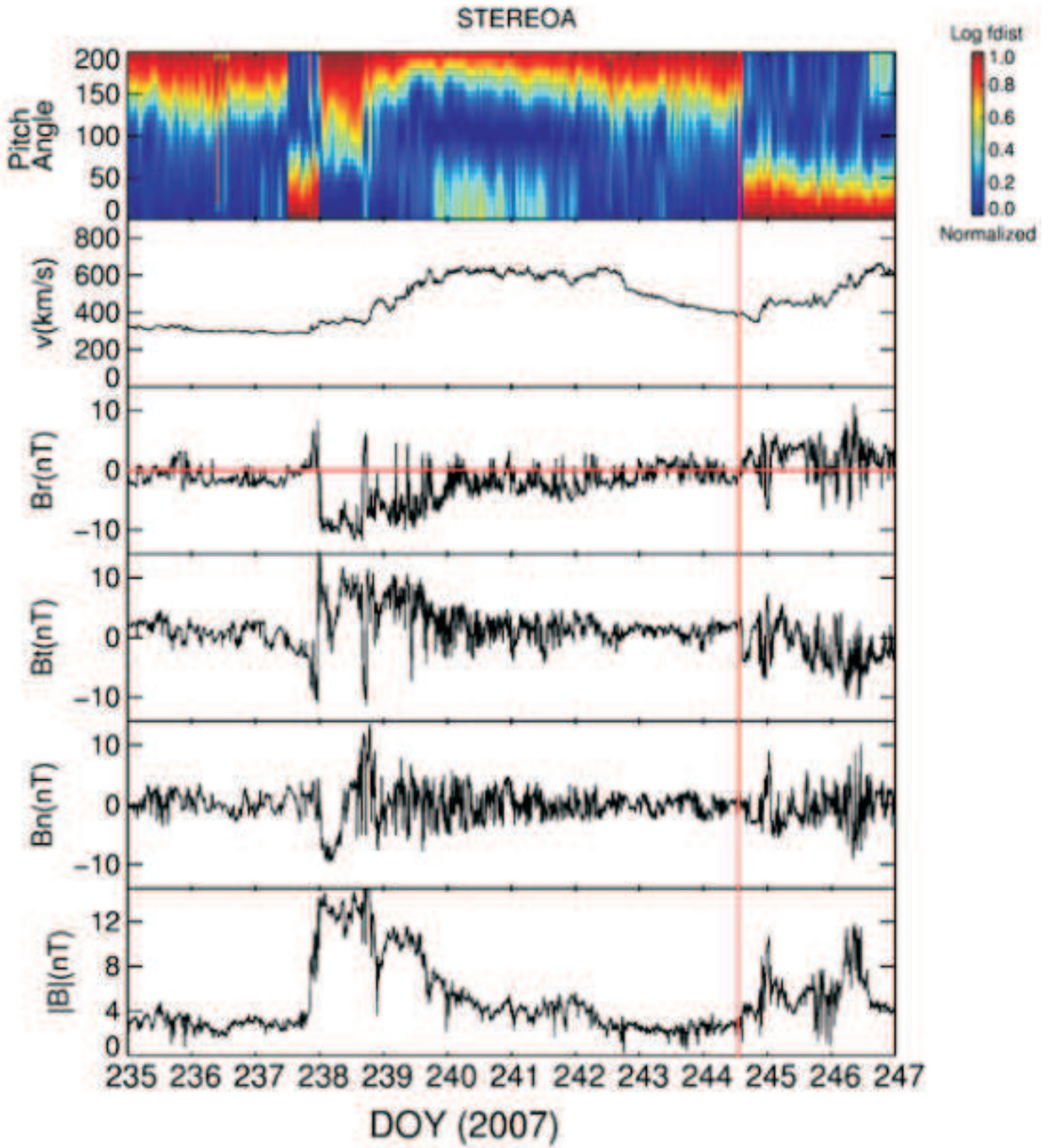


Fig. 11.— Similar to figure 9, but for STEREO-A. Note that the ACE observation uses the GSE coordinate system, while STEREO-A and B use the RTN system. The reversal of  $B_r$  is indicated by the vertical red line.

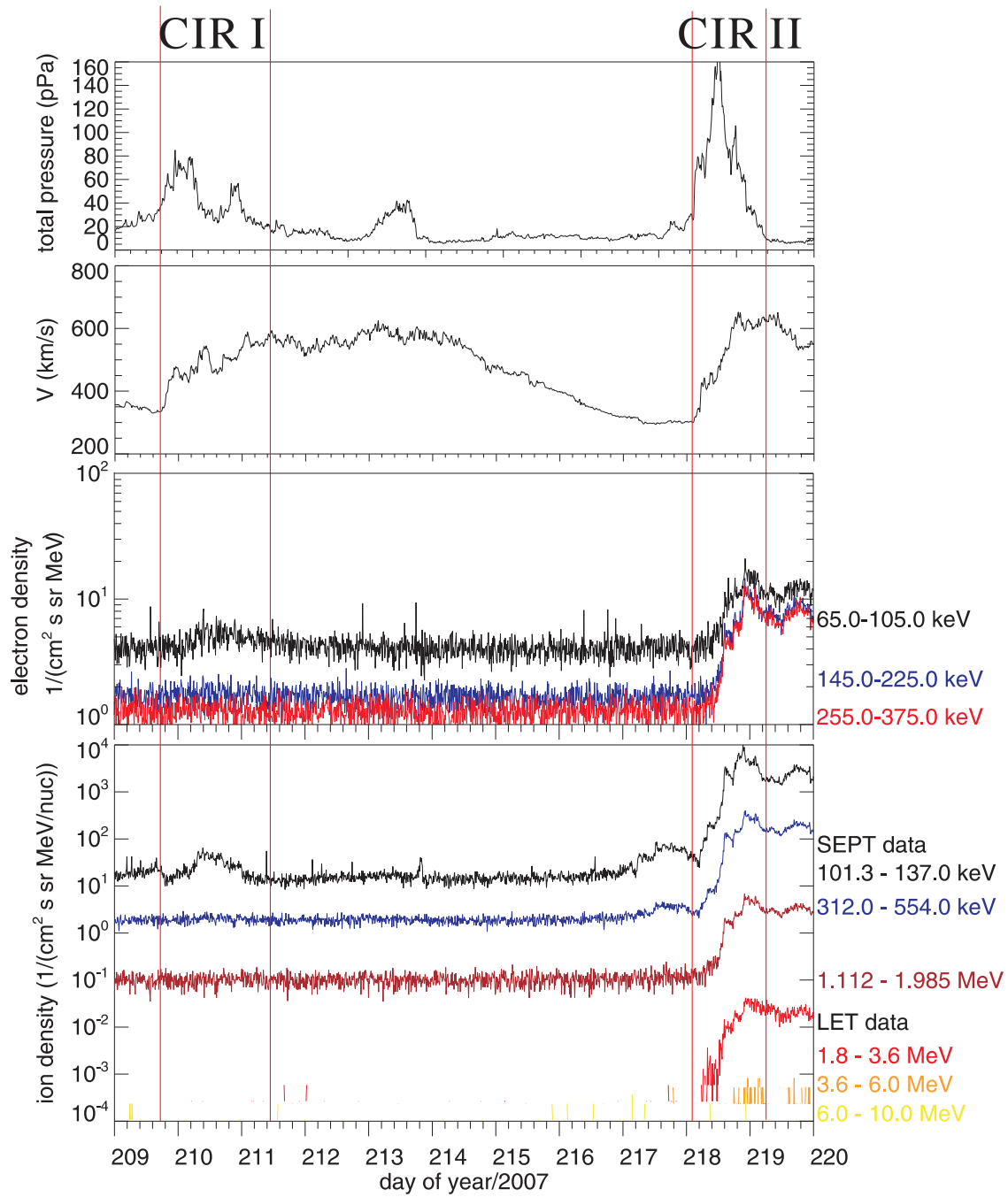


Fig. 12.— CIR pair observation of CR2059. From top to bottom: plasma total pressure, solar wind speed, intensities for energetic electrons (3 energy channels), and intensities for energetic proton and ions (6 energy channels).

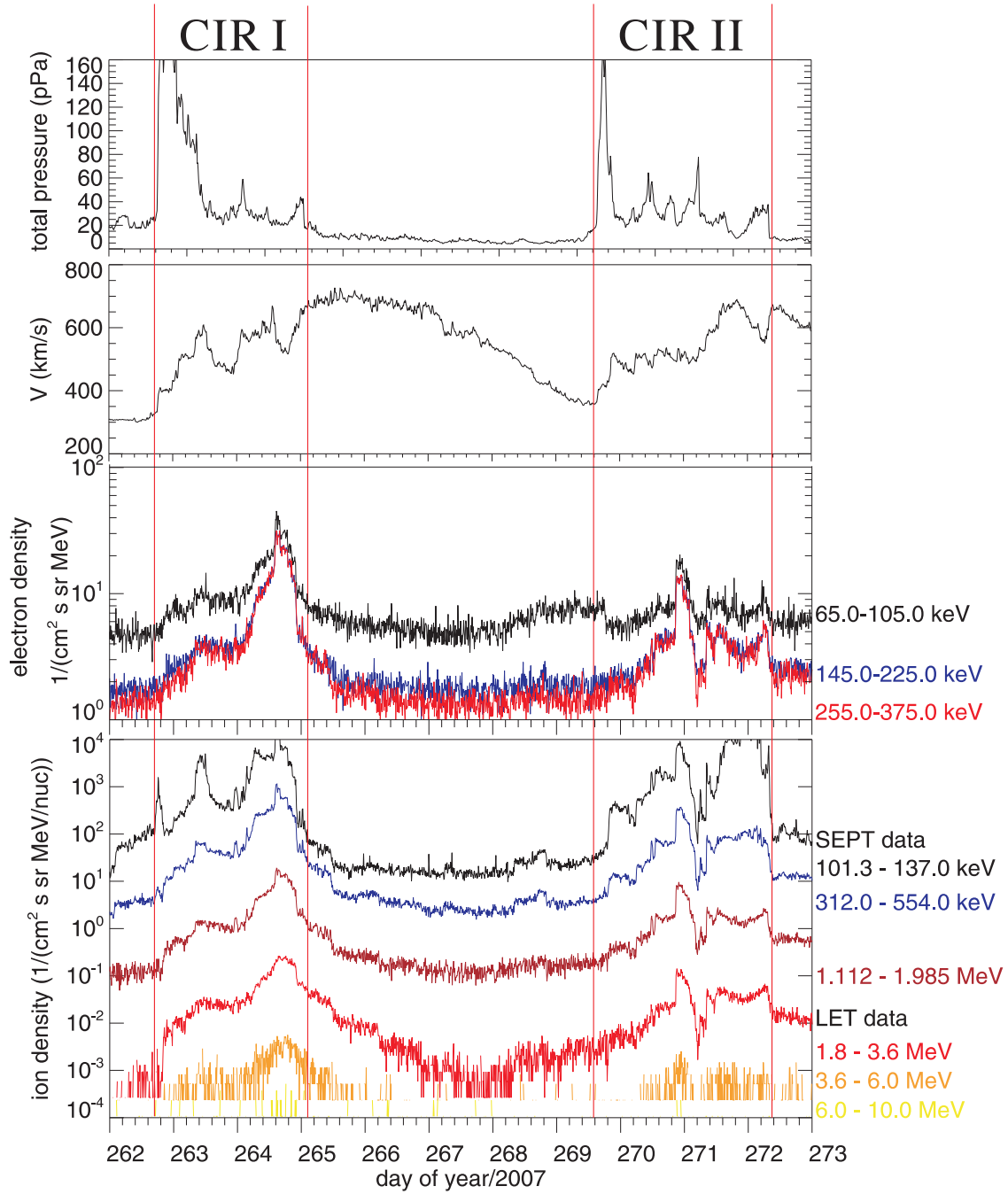


Fig. 13.— Same as Figure 12, but for CR2061.

**REFERENCES**

482

483 Acuña, M. H., Curtis, D. J.L. Scheifele, J.L., Russell, C. T., Schroeder, P., Szabo, A.,  
484 Luhmann, J. G., 2008, Space Sci. Rev., 136, 203

485 Balogh, A. G, Gosling, J.T., Jokipii, J. R., Kallenbach, R., Hunow, H., 1999, Space Sci.  
486 Rev., 89

487 Barnes, C.W. & Simpson, J. A., 1976, APJL, 210, 91

488 Belcher, J. W. & Davis Jr., L., 1971, J. Geophys. Res., 76, 3534

489 Bučík, R., Mall, U., Korth, A., Mason, G. M., 2009, Ann. Geophys., 27, 3677

490 Bučík, R., Gómez-Herrero, R., Korth, A., Mall, U., Mason, G. M., 2009, Solar Phys, 259,  
491 361.

492 Burlaga, L. F., 1975, Space Sci. Rev., 17, 237

493 Chen, Y., Li, X., Song, H.Q., Shi, Q.Q., Feng, S.W., Xia, L.D., 2009, ApJ, 691, 1936

494 Desai, M. I., Marsden, R. G., Sanderson, T. R., et al. 1998, J. Geophys. Res., 103, 2003

495 Dresing, N., Gómez-Herrero, R., Heber, B., et al. 2009, Solar Phys, 256, 409

496 Ebert, R. W., Dayeh, M. A., Desai, M. I., Mason, G. M., 2012, APJ, 749, 73

497 Feldman, W. C., Asbridge, J. R., Bame, S. J., et al. 1981, J. Geophys. Res., 86, 5408

498 Fisk, L. A, 1976, J. Geophys. Res., 81, 4641

499 Fisk, L. A. & Lee, M., 1980, APJ, 237, 620

500 Fisk, L. A., & Jokipii, J. R. 1999, Space Sci. Rev., 89, 115

501 Galvin, A. B., Kistler, L. M., Popechi, M. A., et al., 2008, Space Sci. Rev., 136, 437

- 502 Giacalone, J., Jokipii, J. R., Kóta, J., 2002, APJ, 573, 845
- 503 Gloeckler, G., Jokipii, J. R., Giacalone, J., Geiss, J., 1994, GRL, 21, 14, 1565
- 504 Gold, R. E., Krimigis, S. M., Hawkins, S. E. III., et al., 1998, Space Sci. Revs., 86, 541.
- 505 Gómez-Herrero, R., Klassen, A., Müller-Mellin, R., et al., 2009, J. Geophys.Res., 114,  
506 A05101
- 507 Gosling, J. T., in Physics of Magnetic Flux Ropes, Geophys. Monograph, No. 58, edited by  
508 C. T. Russell, E. R. Priest, and L. C. Lee, AGU, 343, 1990.
- 509 Gosling, J. T., Baker, D. N., Bame, S. J., Feldman, W. C., Zwickl, R. D., and Smith, E. J.,  
510 J. Geophys. Res., 92, No. A8, 8519, 1987.
- 511 Gosling, J. T., Bame, S. J., Feldman, W. C., McComas, D. J., Phillips, J. L., and Goldstein,  
512 B. E., 1993, Geophys. Res. Lett., 20(21), 2335.
- 513 Gosling, J. T., Borrini, G., Asbridge, J.R., et al., 1981, J. Geophys. Res, 86, 5438
- 514 Gosling, J. T., McComas, D. J., Skoug, R. M., and Smith, C. W., Geophys. Res. Lett., 33,  
515 L17102, doi:10.1029/2006GL027188, 2006.
- 516 Gosling, J. T., & Pizzo, V. J. 1999, Space Sci. Rev., 89, 21
- 517 Heber, B., Sanderson, T. R., Zhang, M., 1999, Adv. Space Res., 23, 3, 567
- 518 Hu, Y. Q., 1993, J. Geophys.Res., 98, A8, 13201
- 519 Hu, Y. Q., Chen, J., Zhang, G., 1998, ChA&A, 22, 1, 69
- 520 Hu, Y. Q. & Jia, X. Z., 2001, J. Geophys.Res., 106, A12, 29299
- 521 Jian, L, Russel, C. T., Luhmann, J. G., Skoug, R. M., 2006, Solar phys., 259, 345

- 522 Jokipii, J. R., 2001, Proc. 27th Int. Cosmic Ray Conf. 9, 3581
- 523 Kahler, S., and Lin, R. P., Geophys. Res. Lett., 21, 1575, 1994.
- 524 Krieger, A. S, Timothy, A. F., Roelof, E. C., 1973, Solar phys, 29, 505
- 525 Lavraud, B., Gosling, J. T., Rouillard, A. P., et al., Solar Phys., 256, 379-392, 2009.
- 526 Lavraud, B., Opitz, A., Gosling, J. T., et al., 2010, Ann. Geophys., 28, 233
- 527 Y. Li, J. G. Luhmann, T. Mulligan, J. T. Hoeksema, C. N. Arge, S. P. Plunkett, O. C. St.  
528 Cyr, 2001, J. Geophys. Res., 106, 25103.
- 529 Li, G., Zank, G. P., Rice, W. K. M. 2003, JGR, 108, 1082
- 530 Li, G., Zank, G. P., Rice, W. K. M. 2005, JGR, 110, A06104
- 531 Luhmann, J. G., Gosling, J. T., Hoeksema, J. T. and Zhao, X., 1998, J. Geophys. Res.,  
532 103, 6585.
- 533 Luhmann, J. G., Curtis, D. W., Schroeder, P., et al., 2008, Space Sci. Rev., 136, 117
- 534 McComas, D. J., Bame, S. J., Barker, P., et al., 1998, Space Sci. Rev., 86, 563
- 535 Macdonald, F. B. & Desai, U. D., 1971, J.Geophys.Res., 76, 808
- 536 Mason,G.M., Mazur, J. E.,Dwyer, J. R., et al., 1997, ApJ, 486, L149
- 537 Mason, G. M., & Sanderson, T. R. 1999, Space Sci. Rev., 89, 77
- 538 Mason, G. M., Dwyer, J. R., Mazur, J. E., 2000, APJ, 545, 2, L157
- 539 Mason, G. M., Leske, R. A., Desai, M. I., et al., 2008, APJ, 678, 1458
- 540 Mason, G. M., Korth, A.,Walpole, P. H., 2008, Space Sci. Rev., 136, 257

- 541 Mason, G.M., Desai, M.I., Mall, U., et al., 2009, *Solar phys.*, 256, 393
- 542 Mason, G. M., Desai, M. I., Li, G., 2012, *APJL*, 748, 31
- 543 Mazur, J. E., Mason, G. M., Klecker, B., et al., 1993, *APJ*, 404, 810
- 544 McComas, D. J., Bame, S.J., Barker, P., et al., 1998, *Space Sci. Rev.*, 86, 563
- 545 Mewaldt, R. A., Cohen, C. M. S., Cook, W. R., 2008, *Space Sci. Rev.*, 136: 285
- 546 Möbius, E., Morris, D., Popecki, M. A., et al, 2002, *GRL*, 29, 2, 1
- 547 Müller-Mellin, R., Bottcher, S., Falenski, J., et al., 2008, *Space Sci. Rev.*, 136: 363
- 548 Philipp, W. G., Miggenrieder, H., Montgomery, M. D., Mühlhäuser, K.-H., Rosenbauer, H.,  
549 and Schwenn, R., *J. Geophys. Res.*, 92, 1093, 1987.
- 550 Pizzo, V., 1978, *J. Geophys. Res.*, 83, 5563
- 551 Pizzo, V. J., 1985, in B. T. Tsurutani and R. G. Stone (eds.), *Collisionless Shocks in*  
552 *the Heliosphere: Reviews of Current Research*, Geophysical Mono. No. 35, Amer.  
553 Geophys. Union, 51
- 554 Richardson, I. G., Mazur, J. E., Mason, G. M., 1998, *J. Geophys. Res.*, 103(A2), 2115.
- 555 Richardson, I. G. 2004, *Space Sci. Rev.*, 111, 267
- 556 Sauvaud, J. A., Larson, D., Aoustin, C., et al, 2008, *Space Sci. Rev.*, 136, 227
- 557 Scholer, M., 1999, *Space Sci. Rev.*, 89, 105
- 558 Skoug, R. M., Gosling, J. T., McComas, D. J., Smith, C. W., and Hu, Q., *Suprathermal*  
559 *electron 90 pitch angle depletions at reverse shocks in the solar wind*, *J. Geophys.*  
560 *Res.*, 111, A01101, 2006.

- 561 Simnett, G. M., & Roelof, E. C., 1995, *Space Sci. Rev.*, 72, 303
- 562 Simnett, G. M., 2003, *Adv. Space Res.*, 31, 4, 883
- 563 Smith, C. W., Heures, J. L., Ness, N. F., et al., 1998, *Space Sci. Rev.*, 86, 613.
- 564 Smith, E. J., & Wolfe, J. H., 1976, *Geophys. Res. Lett.*, 3, 3, 137
- 565 Steinberg, J. T., Gosling, J. T., Skoug, R. M., and Wiens, R. C., Suprathermal electrons in  
566 high-speed streams from coronal holes: Counterstreaming on open field lines at 1  
567 AU, *J. Geophys. Res.*, 110, A06103, doi:10.1029/2005JA011027, 2005.
- 568 Tsurutani, B. T., Smith, E. J., Pyle, K. R., Simpson, J. A., 1982, *J. Geophys. Res.*, 87, 7389
- 569 van Hollebeke, M. A. I., McDonald, F. B., Trainor, J. H., von Roseninge, T. T., 1978, *J.*  
570 *Geophys. Res.*, 83, 4723
- 571 van Hollebeke, M. A. I., et al., 1981, *Proc. Solar Wind Conf.* 4, ed. H. Rosenbauer  
572 (Garching: Max-Planck-Institute fur Aeronomie), 497
- 573 Verkhoglyadova, O.P., Li, G., Zank, G. P., Hu, Q., Cohen, CMS, Mewaldt, R.A., Mason,  
574 G. M., Haggerty, D. K., von Roseninge, TT, Looper, MD, 2010, *J. Geophys. Res.*  
575 115, A12103